

Contents lists available at ScienceDirect

Materialia

journal homepage: www.elsevier.com/locate/mtla



Full Length Article

Atomistic simulations and theoretical modeling of dislocation slip and yield response of industrial tantalum alloys



Divya Singh*, Satish I. Rao, Jaafar A. El-Awady*

Department of Mechanical Engineering, Whiting School of Engineering, The Johns Hopkins University, Baltimore, USA

ARTICLE INFO

Keywords:
Dislocation mobility
BCC alloys
Ta-W alloys
Screw and edge dislocations
Solid solution strengthening

ABSTRACT

Dislocation core structure, critical resolved shear stress (CRSS) and mobility of $\frac{1}{2}$ <111> screw and edge dislocations in BCC Ta-8%W alloy was studied using molecular statics and dynamics simulations at 5 and 300 K. Two EAM potentials are available to study the Ta-W system - Johnson-Zhou and Chen potentials. Both potentials give good estimates of edge dislocation mobility in Ta and Ta-8%W. However, the Johnson-Zhou potential predicts a considerably higher CRSS for screw dislocations in pure Ta as compared to experiments. Thus, only the Chen potential is used to study solid solution strengthening in Ta-8%W alloy. The CRSS for Ta-8%W alloy with Chen potential was estimated to be 600 MPa and 300 MPa for screw dislocations at 5 and 300 K, respectively. Edge dislocations exhibit twinning-anti twinning asymmetry in CRSS given the asymmetry in atomic disregistry and dislocation misfit across the glide plane. The simulation results for screw and edge dislocation mobility were found to be in good agreement with the CRSS values from the analytical model of Rao and Suzuki for screw dislocations and the model of Maresca and Curtin for edge dislocations. The study of stability and expansion of shear dislocation loops revealed that theoretical results for loop stabilizing stress from Scattergood and Bacon's equation agreed with results from direct atomistic simulations. The current work predicts that screw dislocations control the experimental yield behavior of the Ta-8at%W alloy at all temperatures. The CRSS for Ta-8%W alloy is a result of solid solution strengthening due to randomly dispersed W solutes in Ta.

1. Introduction

Ta based alloys are of significant interest for high temperature space and nuclear applications. These alloys demonstrate outstanding strength as well as improved corrosion and creep properties at high temperature. However, the mechanical and fracture properties of these alloys are not fully characterized. The use of these Ta based alloys for high-power space nuclear mission have been restricted due to lack of insight into their plastic behavior that govern their mechanical properties.

Plastic deformation in metals is governed by dislocation glide. It is also established that the mobility of dislocation is intricately related to their character as well as external factors like thermal fluctuations [1–3]. In FCC materials, both edge and screw dislocations can glide over the same applied stresses with equivalent speeds [3,4]. However, in conventional BCC metals the energy barrier for a screw dislocation is much larger than that for edge dislocations and therefore slip in these materials is primarily governed by screw dislocations [2–5]. Contrast to this belief, in some new age complex concentrated BCC alloys, both edge and screw dislocations play a significant role in determining the crystal strength [1]. This happens due to the presence of a large amount of random alloying elements, which creates a rugged atomic and energy

profile. These atomic profiles can pin the edge dislocations and thus restrict their motion. Thus, core structure of the dislocations and their glide through the crystal is closely dependent on the local atomic environment. However, it is difficult to study these dislocations at the atomistic level using current experimental methodologies. Therefore, accurate modeling of the alloy system using appropriate interatomic potentials and MD can be key to understanding the local atomic structure and phenomenon that drive dislocation structure, its glide and ultimately the strength of these alloys. The critical information drawn from these simulations can be used to develop and test a wide variety of Ta based alloys with improved mechanical properties.

In this work, atomistic simulations are utilized to predict the core structure, CRSS and mobility of $\frac{1}{2} \ \langle 111 \rangle$ screw and edge dislocations in BCC Ta and Ta-8%W. The accuracy of any MD based simulations depends on the fidelity of the interatomic potential. Thus, we first interrogate two different embedded atom potentials (Zhou and Chen) in terms of the screw and edge dislocation core structures and their CRSS at 5 and 300 K in pure Ta to validate the accuracy of these potentials for the current work. We also use an analytical model for solution strengthening in BCC alloys given by Rao et al. [6] to estimate the CRSS of screw dislocations in Ta alloys considered in this work. The strengthening of edge dis-

E-mail addresses: dsingh44@jh.edu (D. Singh), jelawady@jhu.edu (J.A. El-Awady).

^{*} Corresponding authors.

locations in these alloys is predicted theoretically by employing solute strengthening model given by Maresca and Curtin [7]. A good agreement is found among the existing experimental data on yield strength, the current MD results, and theoretical predictions of the CRSS in the Ta-8%W alloy. In addition, we also explore the shape, stability and expansion phenomenon of dislocation loops as a function of addition of alloying elements in Ta using atomistic simulations.

2. Atomistic simulations methodology

All molecular dynamics simulations conducted here were carried out using the open source code LAMMPS [8]. The EAM potential developed by Zhou et al. [9] (termed hereafter the Zhou potential) was used to model pure Ta. The EAM potential developed by Chen et al. [10] (termed hereafter the Chen potential) was employed for modeling both pure Ta and the Ta-8%W alloy.

Post processing of the results were conducted using OVITO [11]. The local defect structures were characterized with the help of common neighbor analysis (CNA), Centro symmetry parameter (CSP) and Coordination analysis (CA). The Burgers vector, dislocation type, and line direction of the dislocations were visualized in OVITO using the dislocation extraction algorithm (DXA). Differential displacement plots were also used to characterize the core of screw and edge dislocations.

The 0 K lattice and elastic constants of pure Ta and Ta-8%W alloy were calculated using a defect free cubic simulation cell having an edge length of \sim 40 nm (a total of \sim 2 million atoms) with the x, y, and z directions aligned along the [100], [010] and [001] crystal directions. Periodic boundary conditions (PBCs) were enforced in all directions. Energy minimization was carried out using the conjugate gradient (CG) algorithm to achieve the most stable structure corresponding to minimum cohesive energy.

The core structures of screw dislocations and their CRSS for pure Ta as well as the Ta-8%W were studied by introducing a screw dislocation in the center of a simulation cell with its x, y, and z axes aligned along [111], [112] and [110] crystallographic directions, respectively. Firstly, a dislocation-free BCC lattice with PBCs along the line direction (x-axis) and non-periodic free boundary conditions along the other two perpendicular directions was generated and then relaxed using the conjugate gradient minimization technique. An 1/2 [111] screw dislocation was then inserted at the center of the simulation cell using its anisotropic elasticity displacement field with its line direction and Burgers vector parallel to the x-axis. The core structures and CRSS of [111] edge dislocations on {110} and {112} planes in pure Ta and Ta-8%W alloy were also studied by inserting them at the center of the simulation cell using their anisotropic displacement field in a similar manner to that of the screw dislocation simulation setup. In case of an edge dislocation lying on the $\{110\}$ plane, an orthogonal simulation cell was created with its x, y, and z axes aligned along the [111], [$\bar{1}\bar{1}2$], and [1 $\bar{1}0$] directions, respectively. For the case of an edge dislocation on the $\{112\}$ plane, the x, y, and zaxes were oriented along the [111], [110], and [112] directions, respectively. In both cases the x-axis is parallel to the Burger's vector direction and the y-axis is parallel to the dislocation line direction. Periodic boundary conditions are employed again in the dislocation line direction, with free boundaries in the other two directions. Similar boundary conditions have been successfully employed in previous MD simulations where critical resolved shear stresses for screw or edge dislocation motion are calculated in FCC and BCC random alloys with success [2,12]. Schematics of the different simulation cells studied here are shown in Fig. 1 and details of each cell size and number of atoms are summarized in Table 1.

After the insertion of each dislocation in its simulation cell, the cell was minimized using a conjugate gradient (CG) algorithm in multiple steps to make sure that the minimizer does not converge prematurely. This gives the CG minimizer a chance to find a more stable configuration if available, by adjusting the atomic coordinates in every possible direction. This robust minimization scheme is adopted to ensure that

Table 1Details of the different simulations

	Dislocation type	Simulation cell size (nm)	Number of atoms
Zhou potential			
Ta	Screw	\sim 60 \times 50 \times 30	4750140
Chen potential			
Ta	Screw	\sim 60 × 50 × 30	4750140
Ta	Edge (110)	\sim 60 × 60 × 30	6326160
Ta	Edge (112)	\sim 60 × 60 × 30	6119058
Ta-8%W alloy	Screw	\sim 60 \times 50 \times 30	5000112
Ta-8%W alloy	Edge (110)	\sim 60 × 60 × 30	6326160
Ta-8%W alloy	Edge (112)	\sim 60 \times 60 \times 30	6333813

the final 0 K configurations attain the structure corresponding to local minimum energy in terms of atom coordinates.

For all MD simulations, the simulation cell was heated up to the desired temperature (5 K or 300 K) and subsequently relaxed for 50 ps under a constant temperature. A default time step of 0.001 ps was employed. At the end of the relaxation run, the simulation cell reaches the target temperature, and the potential energy and simulation cell dimensions reach a steady stable state value. Upon further relaxation, no significant change in potential energy, temperature, or simulation cell dimensions was observed.

For screw dislocation CRSS calculations, a constant shear stress was applied on a 10 Å thick slabs at the two outer surfaces in the z direction [12]. The per atom force in this slab corresponded to the desired shear stress in the direction of the Burger's vector. For edge dislocations CRSS calculations, per-atom forces were applied on 10 Å thick slabs at the two outer surfaces in the z and x directions to ensure that the simulation cell does not rotate during the MD simulations. In order to calculate the CRSS of screw and edge dislocations the shear stress was applied on the simulation box iteratively with sequential bi-sectioning until the minimum stress, where the dislocation can glide continuously and exit the simulation cell within a 500 ps MD simulation, was reached. This stress is defined here as the CRSS for dislocation motion.

The mobility response for shear dislocation loops at 5 K in Ta and Ta-8%W alloy, were also studied. In addition, the static equilibrium stress needed to maintain a non-expanding non-contracting stable dislocation loop at 0 K in Ta-8%W alloys was calculated as a function of the loop radius in the range of 50-100 Å. Firstly, a perfect simulation cell with periodic boundary conditions in all directions was generated in LAMMPS and minimized using CG minimization. The simulation box had edges oriented along the [111] (x-axis), [$\bar{1}\bar{1}2$] (y-axis), and [1 $\bar{1}0$] (z-axis) directions for loops on the {110} plane, and along the [111] (x-axis), [110] (y-axis), and $[11\overline{2}]$ (z-axis) directions for loops on the $\{112\}$ plane. The size of the simulation cell was chosen in such a way that the x and y edges were seven times the radius of the largest initial stable loop under static equilibrium. This is to guarantee that there are no image interactions across the periodic boundaries, even during loop expansion. Accordingly, the lengths of the edges of the simulation cell were set to be 70, 70 and 30 nm along the x, y, and z directions, respectively (i.e., the simulation cell contained ~6 million atoms). Then using the opensource code ATOMSK [13], elastic displacement field corresponding to a shear dislocation loop having $\frac{1}{2}$ [111] Burgers vector on either the {110} or {112} plane was introduced at the center of the cell. Notice that the plane of the dislocation loop is parallel to the xy-plane in both cases, as shown schematically in Fig. 1(d). The data file corresponding to the dislocated crystal generated in ATOMSK [13] was imported back to LAMMPS [8] for further analysis.

The loop equilibrium shear stress was determined by applying a shear stress in the direction of the Burger's vector on the $\{110\}$ or $\{112\}$ glide plane. This was done by straining the simulation box in accordance with the required constant shear stress. The straining was achieved by applying a final displacement or tilt that corresponds to the desired shear strains to the xz face of the original simulation box. This shear stress was

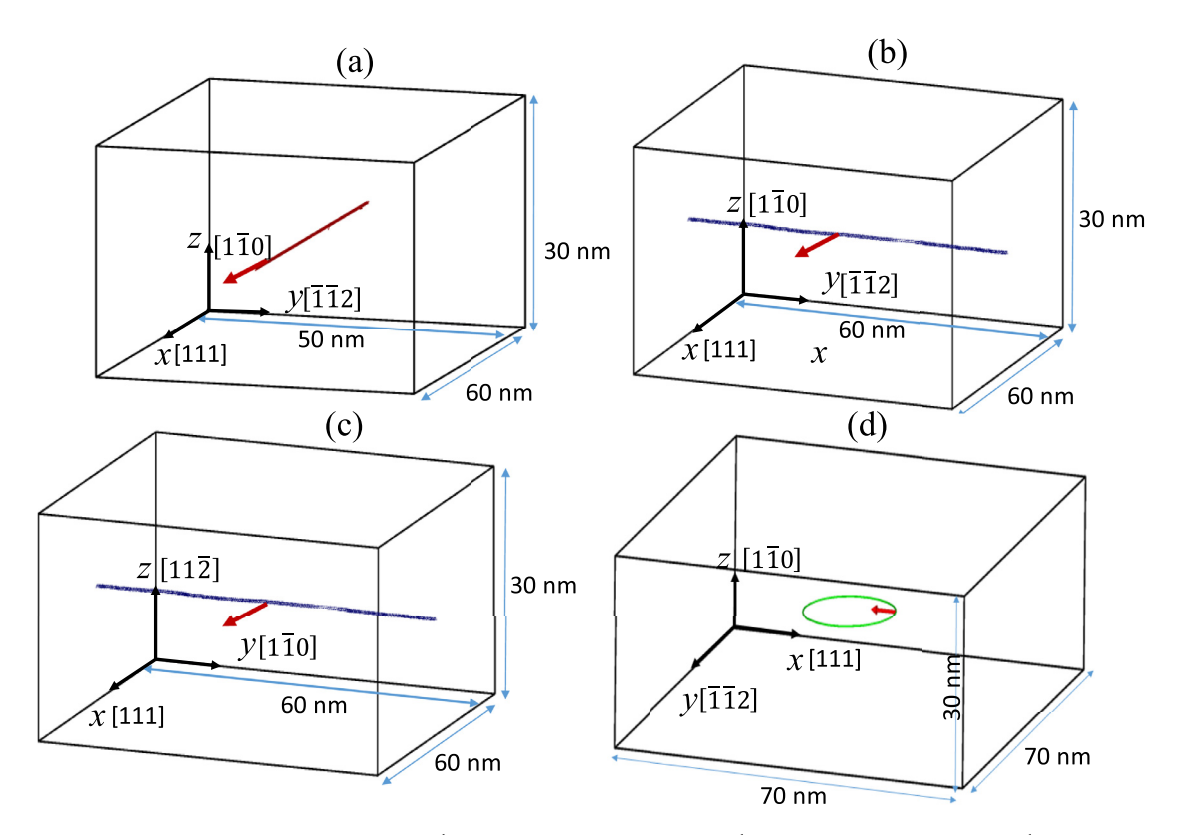


Fig. 1. Schematic of the simulation box containing a central: (a) $\frac{1}{2}[111](110)$ screw dislocation; (b) $\frac{1}{2}[111](110)$ edge dislocation; (c) $\frac{1}{2}[111](112)$ edge dislocation; and (d) $\frac{1}{2}[111](110)$ dislocation loop. The red arrow indicates the direction of the Burgers vector.

estimated using a bisection method in the interval $[0, 2\tau_{theory}]$, where τ_{theory} is the theoretically derived shear stress needed to create a stable dislocation loop. This minimum theoretical stress is given by Scattergood and Bacon as [14]:

$$\tau_{\rm theory} = \frac{G_{\rm A}b}{2\pi 2R_{\rm loop}} \left(\ln \frac{2R_{\rm loop}}{r_{\rm o}} + 1.56 \right) \eqno(1)$$

where $G_{\rm A}$ is the anisotropic shear modulus, b is the Burgers vector of the dislocation loop, $R_{\rm loop}$ is the radius of the dislocation loop, and $r_{\rm o}$ is the dislocation core radius taken to be equal to b. The shear stress application is followed by CG minimisation. The expansion/contraction of the loop during minimization is visualized in OVITO by applying CNA. The stress at which the loop neither expands or collapses during the minimization process, is considered as the loop equilibrium stress.

In order to study the mobility of the dislocation loop at 5 K, firstly a threshold shear stress (above which the loops expand and below which they contract) is estimated at this temperature using MD simulations. In order to achieve this, a pure shear stress was applied in the direction of the Burger's vector on the dislocated simulation cell under a constant temperature at 5 K, in a similar manner to that of 0 K simulation case for static equilibrium case. Further, dynamic evolution of the dislocation loop at 5 K is studied under an applied shear stress greater than this minimum equilibrium stress via MD simulations. The mobility characteristic was then captured using CNA in OVITO.

3. Results and discussion

3.1. Lattice and elastic constants

The predicted lattice constants of pure Ta and Ta-8%W corresponding to the minimum cohesive energy are tabulated in Table 2 obtained from both EAM potentials wherever appropriate. These results are in good agreement with experimental measurements of the lattice constants for pure Ta and Ta-8%W [15–20] as well as with high fidelity

first principle-based density functional theory (DFT) calculations [21–23].

Standard straining methods were used to calculate elastic constants from the defect-free crystals at 0 K. The calculated values of C_{11} , C_{12} and C_{44} corresponding to that of pure Ta and Ta-8%W from different potentials is also shown in Table 2. It is evident from the stated values of the calculated elastic constants that Born stability criteria [24] is satisfied for pure Ta with both potentials as well for the Ta-W alloy with the Chen potential.

3.2. Screw dislocations

3.2.1. The core structure

The differential displacement (DD) plots showing the core structure of a screw dislocation in Ta-8%W alloy, as predicted by the current molecular statics simulations, are shown in Fig. 2. The DD plots are shown at three different locations along the dislocation line to observe the effect of local atomic randomness on the variations in the core structure [25]. The sections chosen for plotting the DD plots are one Burgers vector magnitude, $b = |\mathbf{b}|$, thick perpendicular to the dislocation line direction. Three such sections are taken along the dislocation line at the midpoint and $\pm 50b$ from the midpoint.

Molecular statics simulations using the Chen potential predicts a compact core for the $\frac{1}{2}$ [111] screw dislocation in pure Ta with the dislocation line being centered and straight. This is in agreement with first principles calculations for pure Ta [26]. However, DD plots corresponding to the Ta-8%W alloy at three cross-sections perpendicular to the dislocation line (Fig. 2(a)–(c)) show a split or a 3-fold core structure for the Ta-8%W alloy as well as clear variations in the core structure along the dislocation line direction (Fig. 2(d)). These localized variations along the dislocation line are a result of local atomic fluctuations due the random distribution of solutes. Thus, the DD plots corresponding to the screw dislocation in Ta-8%W alloy indicate that the core structure

Lattice parameter (Å) and elastic constants (GPa) as predicted using the Zhou EAM potential and the Chen EAM potential for Ta, T111, and Ta-8%W. The lattice parameters are in Å and the elastic constants are in GPa

Materials	Materials Lattice parameter	arameter							ئ				Ü				(C., -C.,)/2			
	4				-111-				71-				#				- 1771 - 11-1			
	Zhon	Chen				Chen			Zhou	Chen			Zhou	Chen				Chen		
	EAM	EAM	Exp.	DFT	Zhou EAM	EAM	Exp.	DFT	EAM	EAM Exp.	Exp.	DFT	EAM	EAM	Exp.	DFT	Zhou EAM	EAM Exp.	Exp.	DFT
Ta	3.3021	3.3038	3.303915		263	266	267.9 ²⁰	258.7 ²¹	158	157	162.4^{20}	168.8^{21}	82	87	86.7520	67.8 ²¹	52	55	52.7720	44.9521
			3.3026^{16}	3.308^{22}			266.3^{17}	259.6^{23}			158.2^{20} 165.2^{23}	165.2^{23}			87.417	64.2^{23}			54.05^{17}	47.2^{23}
							266^{18}				160.9^{18}				82.47^{18}				52.53^{18}	
Ta-8%W		3.2749				300	287.98^{20}			164	162.1^{20}			91	62.93^{20}			89	62.93^{20}	

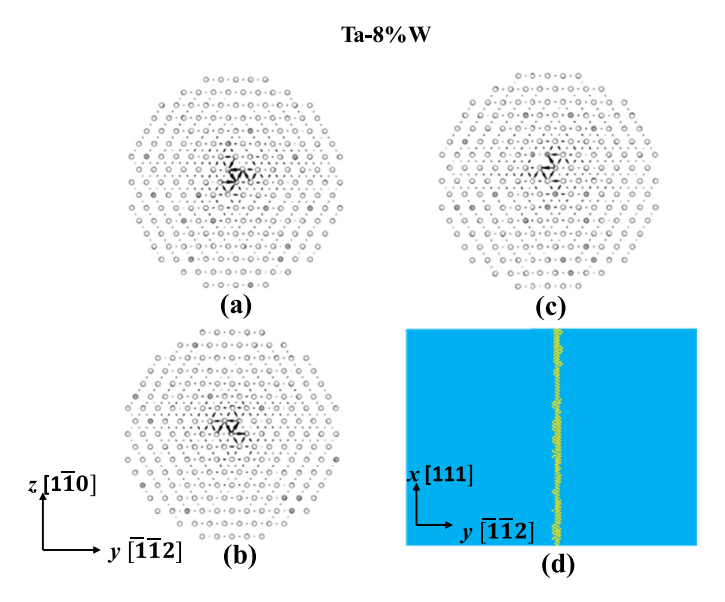


Fig. 2. Differential displacement plots at three sections along the screw dislocation line: (a) 0; (b) 50b; and (c) -50b relative to the midpoint of the dislocation line in Ta-8%W. (d) The corresponding CNA showing only the non BCC atoms of the dislocation core in Ta-8%W.

is characteristically different from those obtained from first principles predictions as well as MS simulations for pure Ta [26] or pure W [27–30].

In continuation with the above discussion, it should be pointed out that atomistic potentials frequently show a metastable split core as a local minimum for the core structure of $\frac{1}{2}$ [111] screw dislocations in BCC structures [31] as we observe here for the Ta-8%W. This could be an artefact of the interatomic potential, since first principles calculations in pure BCC metals does not show the split core as a local minimum for $\frac{1}{2}$ [111] screw dislocations [32]. This is shown here for pure Ta using the Chen EAM potential by varying the initial elastic center of the anisotropic elasticity displacement field used to insert the screw dislocation in the simulation cell, thus, various possible local minimum energy core structures for the $\frac{1}{2}$ [111] screw dislocation can be identified. It is found that a compact core as well as a split core are local minima as shown by the DD plots in Fig. 3. The energy of the compact core is $1.486~{\rm eV/\mathring{A}}$ and that of a split core is $1.458~{\rm eV/\mathring{A}}$.

The relative energies indicate that both the split core and compact cores are local minima, with the split core having a slightly lower energy. The presence of split core as a local minima is an artefact of many well-known BCC potentials in the literature including Mendelev potential for Fe [33] and other potentials for Ta [38-40]. The Chen potential gives the right core structure for pure Ta but the wrong one (asymmetric) for pure W. This is a possible reason for the observed asymmetric core in Ta-8W. Wang et al. [34] employed an empirical EAM interatomic potential that gives an asymmetric dislocation core for screw dislocation in Ta in disagreement with DFT calculations. However, they successfully estimated the Peierls barrier in pure Ta using this potential. Similarly, Ito and Vitek [35] obtained two non-equivalent degenerate cores in Mo using central-force many-body potentials [36] contrary to the symmetric cores found in DFT calculations [37]. Here also, the barrier to dislocation motion was determined successfully. This suggests that the details of the core structure is relatively unimportant on the critical stress level to move screw dislocations, especially in alloys where solute barrier to dislocation motion is of paramount importance. As discussed by Weinberger et al. [31] and later in this manuscript, this split-core structure leads to the preferred glide plane of the screw dislocations being the {112} plane under an applied pure shear stress on the {110} plane. Hale et al. [49] studied various empirical interatomic potentials [38-40] available for Ta for screw dislocation core structure. All the inter-

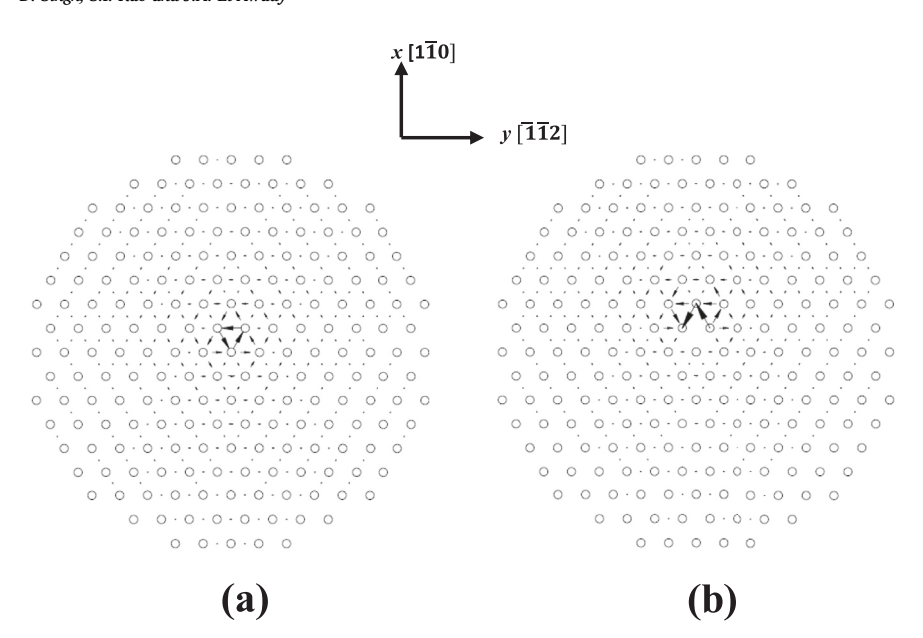


Fig. 3. Two different $\frac{1}{2}$ [111] screw dislocation core configurations in pure Ta obtained using the Chen potential by varying the initial elastic center of the anisotropic elasticity displacement field used to insert the screw dislocation resulting in: (a) a compact core; or (b) a metastable split core.

Table 3 CRSS and velocity of screw dislocations in pure Ta and Ta-8%W at 5K and 300K, using the Zhou and/or Chen potentials. Results from the Rao-Suzuki model for the mobility of $\frac{1}{2}$ [111] screw dislocations in Ta-8%W are also given.

Composition	Temperature	Ta (Zhou potential)	Ta (Chen potential)	Ta-8%W (Chen potential)
CRSS (MPa)	5K	2000	400	600
[MD simulations]	300K	600	150	300
CRSS (MPa)	5K	350 (4.2 K) ^[16]	350 (4.2 K) ^[16]	-
[Experimental]	300K	180 ^[17] (RT) -200 (296 K) ^[18]	180 ^[17] (RT) - 200 (296 K) ^[18]	218 ^[21] 285 (RT) ^[17]
CRSS (MPa)	5K	-	-	629 (MD strain rate)
[Rao-Suzuki				626 (Experimental strain rate)
model]	300K	-	-	426 (MD strain rate)
				288 (Experimental strain rate)

atomic potentials reproduce a split core configuration, which is deemed responsible for the preferred {112} slip of the screw dislocation.

It should also be pointed out that the Chen potential accurately reproduces the much-expected core structure fluctuations along the dislocation line in Ta-8%W alloy [2,12].

3.2.2. The critical resolved shear stress

The critical resolved shear stress (CRSS) for screw dislocations in pure Ta and Ta-8%W alloy as calculated at 5 and 300 K are summarized in Table 3. The dislocation velocity of the continuously gliding dislocations at this CRSS is obtained from the displacement-time plots by fitting a linear curve and are also listed in Table 3.

The estimated CRSS for pure Ta from the Zhou potential are a factor of 3-6 times larger than experimental results as shown in Table 3. This suggests that the Zhou potential cannot be used to study solute effects on the mobility of screw dislocations. On the other hand, the Chen potential predictions for the CRSS of $\frac{1}{2}$ [111] screw dislocations in pure Ta at both 5 and 300 K are in reasonable agreement with experimental predictions. This indicates that the Chen potential can be reasonably used to study W solute effects on the mobility of $\frac{1}{2}$ [111] screw dislocations in Ta-8%W. Atomistic potentials as well as first principles calculations are notorious in predicting a high value of screw Peierls stress for BCC metals at low temperatures (0-5 K) in comparison with experimental yield data [41–43]. Several theories have been proposed for this discrepancy in the literature [33,59]. To evaluate the solute barrier to screw dislocation motion in the Ta-8%W alloy at low temperatures, the original Peierls or kink-pair barrier for screw dislocation motion in pure Ta needs to be as close to experimental data as possible. This ensures that the BCC alloy behavior (for a reasonable concentration of solutes) for screw dislocations is dominated by the solute barrier, Otherwise, in the case of an artificially very high kink-pair barrier for screw dislocation motion in pure Ta, kink-pair barrier effects cloud the alloy results erroneously.

Fig. 4(a) and (b) show a top view of the screw dislocation gliding at 5 K and an applied shear stress of 600 MPa in Ta-8%W. Debris in the form of vacancy and interstitial clusters are observed to form behind the screw dislocation as it glides forward. This debris is a result of activation of multiple cross kinks during the glide process. Cross-kinks are caused by the collision of kinks gliding on different {110} planes. The W-solutes facilitate the nucleation of these kinks on different {110} planes. During the glide process, the screw dislocations drag the cross-kink pinning points to form clusters (vacancy or interstitial like). Every once in a while, clusters pinch-off from the screw dislocation leaving behind the debris shown in the plots. Similar observation of cross-kink induced debris in the wake of screw dislocation in other BCC alloys have also been reported previously [2,5,9,13].

A combination of CNA, CSP and CA was used to identify the vacancy and interstitial clusters, following the methodology proposed by Moller and Bitzek [44]. First CNA filters out all the atoms that do not belong to the perfect BCC lattice, (i.e., screw dislocation and the vacancy and interstitial clusters). In order to differentiate between the screw dislocation and the debris clusters, coordination analysis in OVITO was employed with a cut-off radius of $1.2a_0$, where a_0 is the lattice constant. Atoms with coordination numbers (CN) smaller than 14 can be identified as vacancy clusters, since atoms constructing the screw dislocation have a CN equal to 14. In order to identify the interstitial clusters, a cut-off radius of $\sim 0.8a_0$ was used for coordination analysis in OVITO. At this cut-off, only interstitials have non-zero number of nearest neighbors. Boolean operation was used in OVITO to hide all atoms with CN = 0

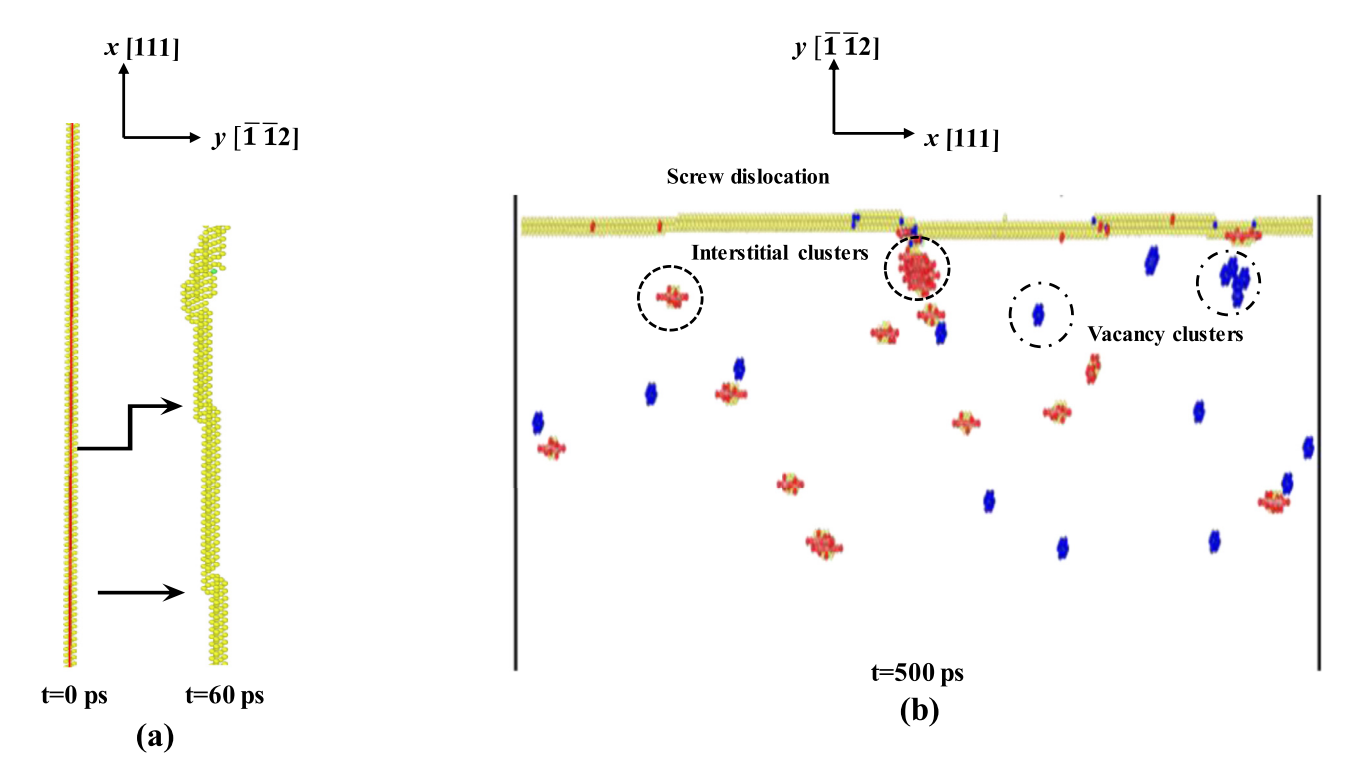


Fig. 4. (a) Two sequential snapshots showing the formation of cross kinks on a screw dislocation in the Ta-8%W alloy during its glide. The applied shear stress is 600 MPa at 5 K. (b) Interstitial and vacancy debris production during $\frac{1}{2}$ [111] screw dislocation glide in a Ta-8%W alloy at 5 K and an applied shear stress of 600 MPa. Atoms belonging to the screw dislocation core are shown in yellow, interstitial clusters in red, and vacancy clusters in blue.

and preserve only the interstitial atoms. Overall, the total number of atoms at the vacancy and interstitial clusters are identical to each other, as expected. Conversely, their distribution in the simulation cell is not identical. We can note from Fig. 4 that the vacancy clusters are visibly smaller in size but greater in number than the interstitial clusters. Similar behavior is observed in the work of Marian et al. [45] where the authors point out that the difference in the size of the vacancy and interstitial clusters is closely related to the difference in vacancy and interstitial formation energies in BCC Fe.

It should be noted that for both pure Ta as well as the Ta-8%W with the Chen potential the screw dislocation consistently glides on the {112} plane. In contrast, published experimental studies indicate that glide on {110} planes dominate in BCC metals, including Ta and its alloys [46–48]. Hale et al. [49] gave a detailed description of how the interatomic potentials may influence the screw dislocation core structure and the glide pathways in Ta. Their study revealed that the effective {112} slip trace observed via MD simulations in Ta is a result of {110} glide on two different planes that alternate through compact and split core positions on the slip pathways. Thus, as previously stated, the preferential slip of the screw dislocations on {112} planes as observed in the current simulations in Ta and Ta-8%W is related to the presence of the metastable split core as a local minimum and is a manifestation of the potential employed in this work.

3.2.3. Theoretical predictions of the CRSS

The Rao-Suzuki model for substitutional solid solution strengthening in BCC alloys is used here to predict the theoretical CRSS of screw dislocations in Ta-8%W and compare it to the MD predictions. The model described in detail elsewhere [50–54], and here, only a brief description of the model is given for completeness. The model considers substitutional solid solution strengthening in BCC alloys to have two contributions: (a) a stress τ_k to move kinks across solute obstacles at the screw dislocation core; and (b) a stress τ_j to bow screw dislocations between interstitial and vacancy dipoles formed on the dislocation line due to kink-kink col-

lisions. Thus, the CRSS τ_y for the motion of a $\frac{1}{2}$ [111] screw dislocation can be decomposed into two contributions [50–54]:

$$\tau_{y} = \tau_{k}(L) + \tau_{j}(L) \tag{2}$$

Both τ_k and τ_j are functions of the unknown spacing, L, defined as half the distance between the dipoles formed on the screw dislocation. The CRSS is thus minimized with respect to L to give the resolved yield stress, τ_v :

$$\delta \tau_{v} / \delta L = 0 \tag{3}$$

The stress τ_j required to bow the screw dislocations between the interstitial and vacancy dipoles can be written as [55]:

$$\tau_j = \frac{E_{\text{vac}} + E_{\text{int}}}{4bL} \tag{4}$$

where $E_{\rm vac}$ and $E_{\rm int}$ are the vacancy and interstitial dipole energy per unit length formed on the screw dislocation during its motion, respectively. Here, $E_{\rm vac}$ and $E_{\rm int}$ are dominated by the core energy and can be expressed in terms of the vacancy and self-interstitial formation energies as $E_{\rm vac} = 0.707 \; \frac{E_{\rm int}^f}{b}$ and $E_{\rm int} = 0.707 \; \frac{E_{\rm int}^f}{b}$, where $E_{\rm v}^f$ and $E_{\rm int}^f$ are the vacancy and interstitial formation energies, respectively. The values of $E_{\rm v}^f$ and $E_{\rm int}^f$ for Ta are taken from published first principle calculation results [56].

Additionally, τ_k is determined from the following 4th order algebraic equation:

$$\tau_k^4 + S\tau_k - R = 0 \tag{5}$$

Where

$$S = \left[\frac{18kT \left(\sum_{i} \left(k_i^2 E_{wi}^2 c_i \right) \right)}{a_p^3 b^4 \Lambda_k^2} \right] * \ln \left[(5\pi kT)^2 v_0 a_p b / \left((\mu b \Delta V)^2 \varepsilon \right) \right]$$
 (6)

$$R = \left[27 \frac{\sum_{i} (k_i^2 E_{wi}^2 c_i)^2}{a_p^4 b^6 \Lambda_k^2} \right]$$
 (7)

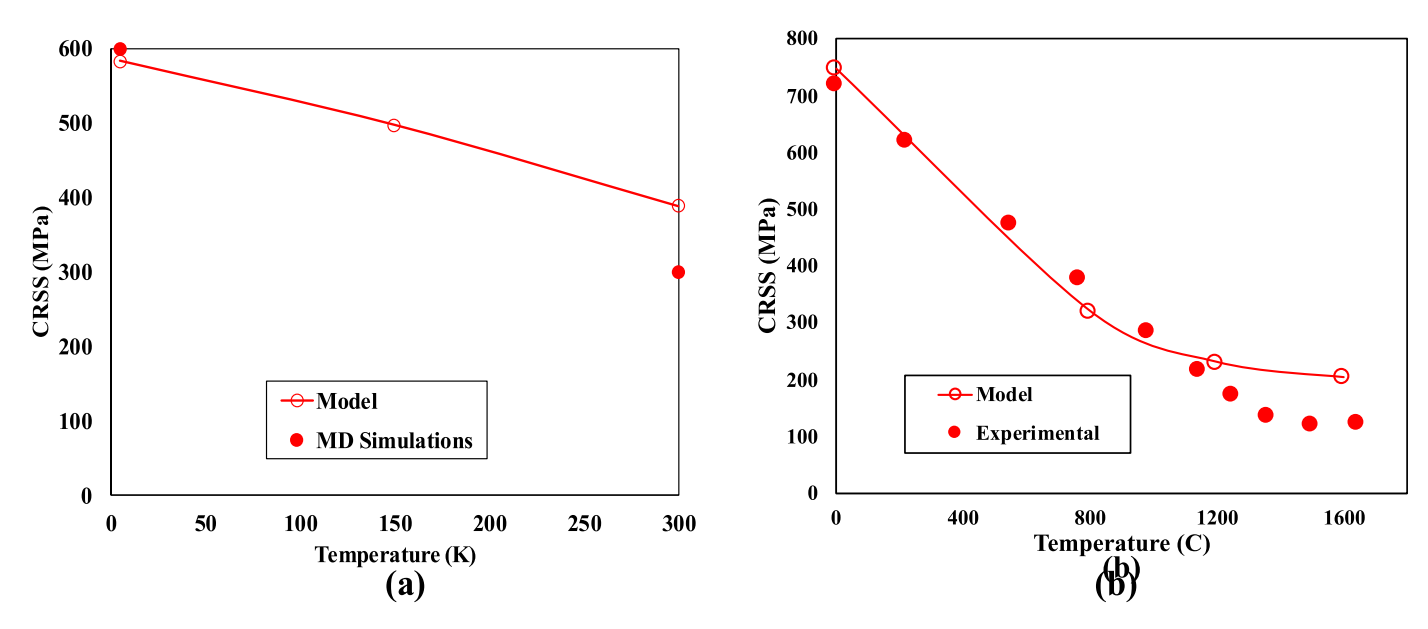


Fig. 5. (a) CRSS for screw dislocations as a function of temperature in the Ta-8%W alloy as predicted from MD simulations using the Chen potential. For the Rao-Suzuki model results, $\delta H(\tau)/kT$ was fixed at 11.5 to mimic MD strain rates. **(b)** The yield strength versus temperature of Ta-10%W as measured experimentally [63] and as predicted using the Rao-Suzuki model.

$$\Delta V = \left[\frac{3(\sum_{i} k_{i}^{2} E_{wi}^{2} c_{i})}{2\tau_{\nu}^{2} a_{p} b^{2}} + (2\tau_{k}^{2} a_{p}^{3} b^{4} \Lambda_{k}^{2} (\sum_{i} (k_{i}^{2} E_{wi}^{2} c_{i})^{-1} \right]$$
(8)

$$\frac{1}{2\pi^{0.5}} \int_{-\infty}^{\infty} k_i \exp\left(\frac{-x^2}{2}\right) dx = \frac{b}{3Lc_i}$$
 (9)

and ΔH , which is the activation energy for kinks to overcome the solute obstacles, is:

$$\Delta H = 3 \frac{(\sum_i k_i^2 E_{wi}^2 c_i)}{2\tau_k a_p b^2} - 0.056 \tau_k^3 a_p^3 b^4 \Lambda_k^2 (\sum_i k_i^2 E_{wi}^2 c_i)^{-1} \eqno(10)$$

In Eq. (6) through Eq. (10), $\Lambda_k \approx 10b$ is the kink width, ΔV is the activation volume for kinks overcoming solute obstacles, $v_0 \approx 5 \times 10^{12} \ \rm s^{-1}$ is the Debye frequency, T is the temperature in Kelvin, k is the Boltzmann constant $\dot{\epsilon}$ is the strain rate, and $E_{\rm wi}$ is the effective solute-screw dislocation interaction energy for solute 'i'. To obtain polycrystalline yield strength, the critical shear stress τ_y is multiplied by a Taylor factor of M=2.75, which is a standard for BCC structures [25].

Thus, to determine solution strengthening due to W solutes in Ta using the Rao-Suzuki model, one requires the W solute-screw dislocation interaction energy (E_w) . The procedure to determine this interaction energy using interatomic potentials is given in Rao et al. [25]. In the current work, as determined for the 6 atom Suzuki model from molecular static simulations using the Chen EAM potential, this energy is E_{w} ~0.20 eV. Previous first principles calculations of W solute-screw dislocation interaction energy in pure Ta show that the interactions extend up to the fourth neighbor (i.e., 27 atoms) [57]. Such fourth neighbor interactions can be mapped onto a 6 neighbor Suzuki model, using an effective interaction energy, as described in Rao et al. [25]. The first four neighbor W solute-screw dislocation interaction energies for W solute in pure Ta has been previously determined from first principles calculations and the effective interaction energy calculated from these values is ~0.15 eV [58]. Thus, a comparison of the effective W solutescrew dislocation interaction energy in pure Ta as determined from first principles calculations ($E_w \sim 0.15$ eV) with those using the Chen EAM interatomic potential in our current work ($E_w \sim 0.20$ eV) shows that the agreement is satisfactory, though not exact.

The CRSS for the Ta-8at% W alloy as determined from the current MD simulations at 5 and 300 K using the Chen potential as well as those predicted based on the Rao-Suzuki model using an effective interaction

energy of 0.20 eV are shown in Fig. 5(a). Both the results are shown to be in good agreement with each other. MD strain rates were employed in the Rao-Suzuki model to achieve this correspondence. Fig. 5(b) compares the Rao-Suzuki model results with experimental data for the yield strength of Ta-10%W in the temperature range 300–1873 K. The Rao-Suzuki model used an effective interaction energy for W solutes in pure Ta as determined from first principles calculations [57]. The agreement between the experimental measurements and the model over this large temperature range is in general agreement. For theoretical estimates of CRSS to compare against experimental values, an experimental strain rate of $10^{-3} \, \rm s^{-1}$ was used in all the analytical calculations.

3.3. Edge dislocations

3.3.1. The core structure

The predicted DD plots of the cross-section as well as top views of the relaxed configuration of the $\frac{1}{2}$ [111]{110} and $\frac{1}{2}$ [111]{112} type edge dislocations on their glide plane as predicted using the Chen potential in pure Ta and Ta-8%W are shown in Fig. 6. The DD plots indicate planar spreading of the edge dislocations on their glide plane for both pure Ta and Ta-8%W, which is an expected behavior for edge dislocations in elemental BCC metals [2,12]. It is also interesting to note that while the edge dislocation remains straight in pure Ta, the dislocation line in the Ta-8%W alloy is wavy. A long edge dislocation in BCC materials is quite flexible unlike the screw dislocation core [7] as the line tension of the edge dislocation is theoretically smaller than that of screw dislocation. In a random BCC alloy, local variation in solute concentration leads to regions of high and low energies. Given the flexibility in dislocation line, the edge dislocation adopts a wavy configuration as it gets attracted to fluctuations that decrease the overall energy of the system, while being repelled from the fluctuations that increase the energy. The waviness has a characteristic wavelength, which is constrained by the line tension of the dislocation or the energy cost of increasing the dislocation line length and curvature. Such localized fluctuations are absent in pure BCC Ta, and hence this characteristic waviness is only observed in the case of Ta-8%W. Maresca and Curtin [7] implement this in a theoretical model that defines a characteristic wavelength, amplitude, and lateral length of the edge dislocation in random BCC/FCC alloys, which appears as a result of energy and line tension constraints on the dislocation line.

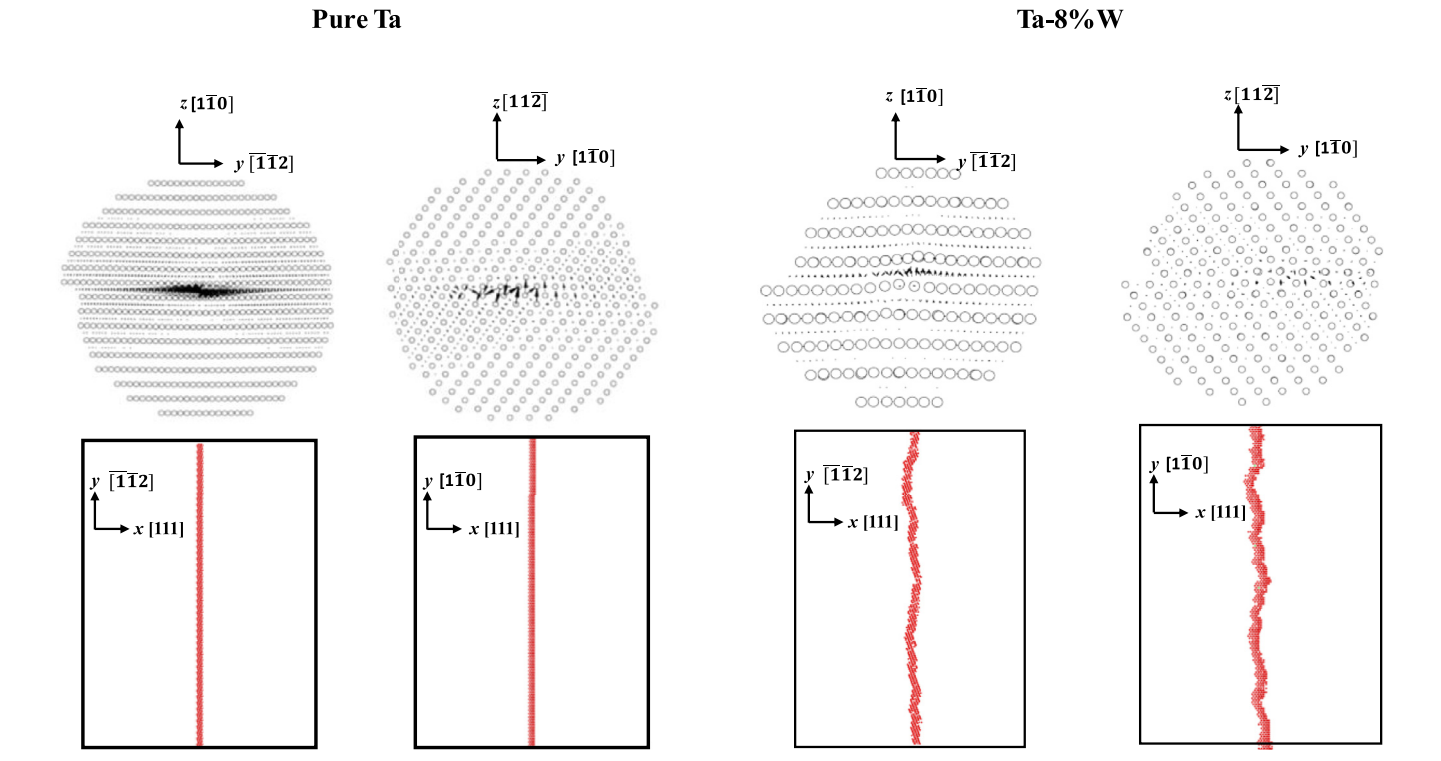


Fig. 6. DD plots (top row) and CNA extract (bottom row) of the corresponding dislocation cores showing only non BCC atoms for the $\frac{1}{2}$ [111] (110) and $\frac{1}{2}$ [111](112) edge dislocations in (a) and (b) for pure Ta and in (c) and (d) for the Ta-8%W alloy.

(b)

Similar observation for an edge dislocation has been made by Rao and coworkers in other BCC alloys [25].

(a)

Additionally, the DD plots for both types of edge dislocations show asymmetry in the core structure. Thus, it is expected that the CRSS for the motion of edge dislocations in the positive and negative sense for both types of edge dislocations in pure Ta and Ta-8%W will be asymmetric. This is commonly referred to as twinning direction (TD) and anti-twinning direction (AD) asymmetry. This will be discussed in the following subsection in details.

3.3.2. Atomic disregistry and differential misfit of edge dislocations in pure Ta

A generalized Peierls–Nabarro (PN) model [58,59] represents the core structure of an edge dislocation in terms of displacement distribution just above and below the dislocation plane. The absolute values of displacements in the upper and lower {112} and {110} planes due to the introduction of an edge dislocation in a perfect pure Ta crystal (i.e., the difference in atomic positions in a relaxed crystal containing an edge dislocation versus that of a perfect crystal), in the direction of the Burger's vector, as predicted from the current molecular static simulations using the Chen potential are shown in Figs. 7 and 8, respectively. Additionally, the disregistry density (or differential misfit) corresponding to the absolute displacements is also determined and shown in Figs. 7 and 8.

It is observed that the absolute values of the displacement evolution above (upper layer) and below (lower layer) the dislocation plane are not identical for the {112} plane. This is evident from the asymmetry in the disregistry and differential misfit plots in Fig. 7(b)–(e). This asymmetry around the core of an edge dislocation causes anisotropy in the atomic forces in the twinning and anti-twinning directions in both pure Ta and Ta-8%W and leads to differences in the CRSS required to initiate dislocation glide in the TD and AD. Interestingly, similar observations have also been made for $\frac{1}{2}$ [111] (112) edge dislocations in pure Fe [60].

3.3.3. The critical resolved shear stress

(c)

The CRSS for an edge dislocation in pure Ta and Ta-8%W are first calculated using MD simulations. The evaluated CRSS for $\frac{1}{2}$ [111] {110} and {112} edge dislocations at both 5 and 300 K are summarized in Table 4. The CRSS for $\frac{1}{2}$ [111] edge dislocations in pure BCC Ta estimated with the Chen potential at 5 K varies between 5 and 35 MPa based on the habit plane. However, for the {110} edge dislocation in pure Ta, no asymmetry in the CRSS for moving the edge dislocation was observed in the AD or TD directions. This is in agreement with the symmetric atomic disregistry curves in pure Ta for the {110} plane as shown in Fig. 7(b) and (d). In the case of $\frac{1}{2}$ [111]{112} edge dislocations, a small asymmetry in the CRSS was observed in the AD and TD. This is in agreement with the asymmetry in the differential misfit plots corresponding to the {112} plane in pure Ta as shown in Fig. 8(b) and

(d)

From the values summarized in Table 4, it can be observed that the edge dislocations in Ta-8%W lying on the {110} and {112} planes show an asymmetry in the CRSS when the sign of the shear stress is reversed, which again can be attributed to the asymmetric evolution of atomic disregistry and differential misfit in the TD and AD. It is also interesting to note that the CRSS for the $\frac{1}{2}$ [111]{110} and $\frac{1}{2}$ [111]{112} edge dislocations in both pure Ta and Ta-8%W are also different given the significant difference in core structures of both types of edge dislocation. It can be seen from Figs. 6, 7(a) and 8(a) that the {110} edge dislocation has a spread-out core, while the {112} edge dislocation displays a comparatively compact core. This results in a difference in the edge dislocation core-solute interaction energies for the two types of dislocations that eventually manifests as the difference in the CRSS on the {110} and {112} edge dislocations. The W solute-edge dislocation interaction energies in bulk Ta as predicted from the current molecular static calculations is -0.19 and 0.4 eV above and below the cut plane in case of {110} edge dislocations. For the {112} edge dislocation this value was estimated as -0.53 eV.

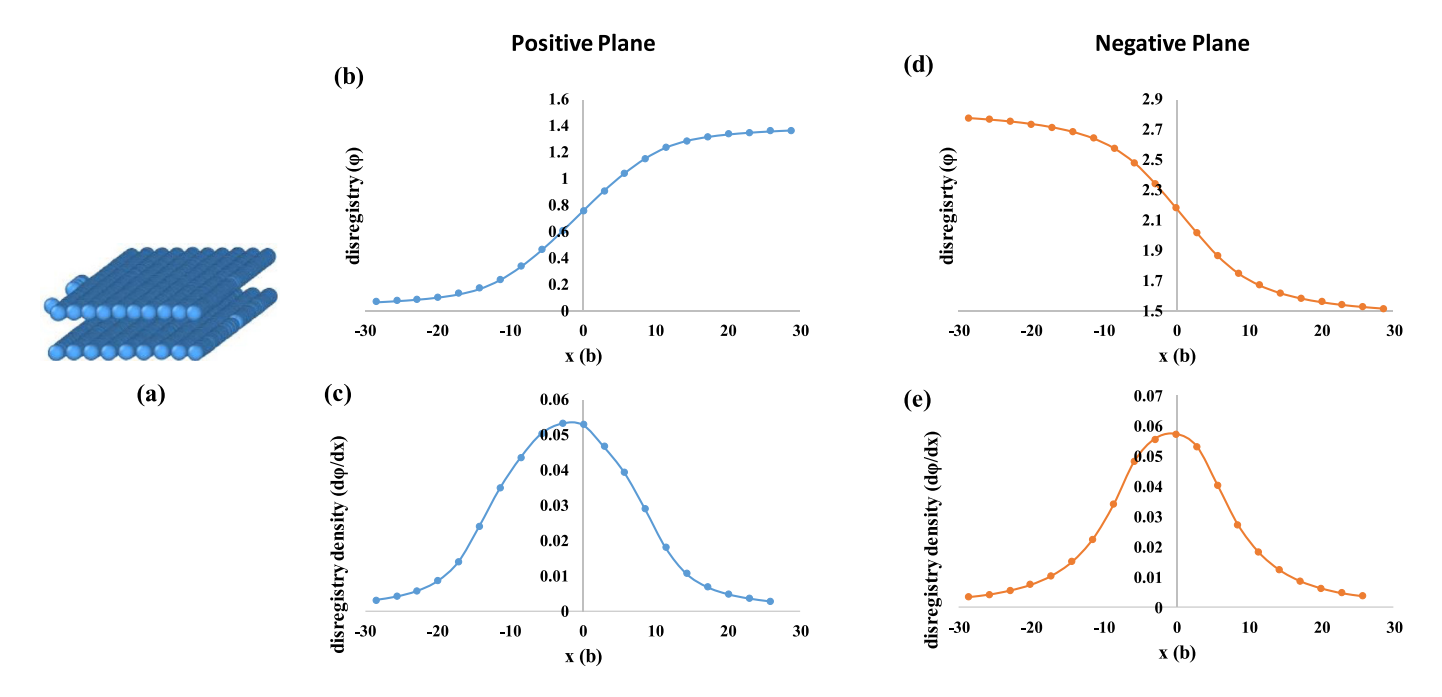


Fig. 7. (a) The core structure of $\frac{1}{2}$ [111] edge dislocations on the {110} plane and the corresponding atomic disregistry plots (or displacement functions) for this edge dislocation in units of b of atomic layers immediately: (b) above (upper layer) and (d) below (lower layer) the (110) slip plane and their corresponding differential misfit plots: (c) above (upper layer) and (e) below (lower layer) the (110) slip plane.

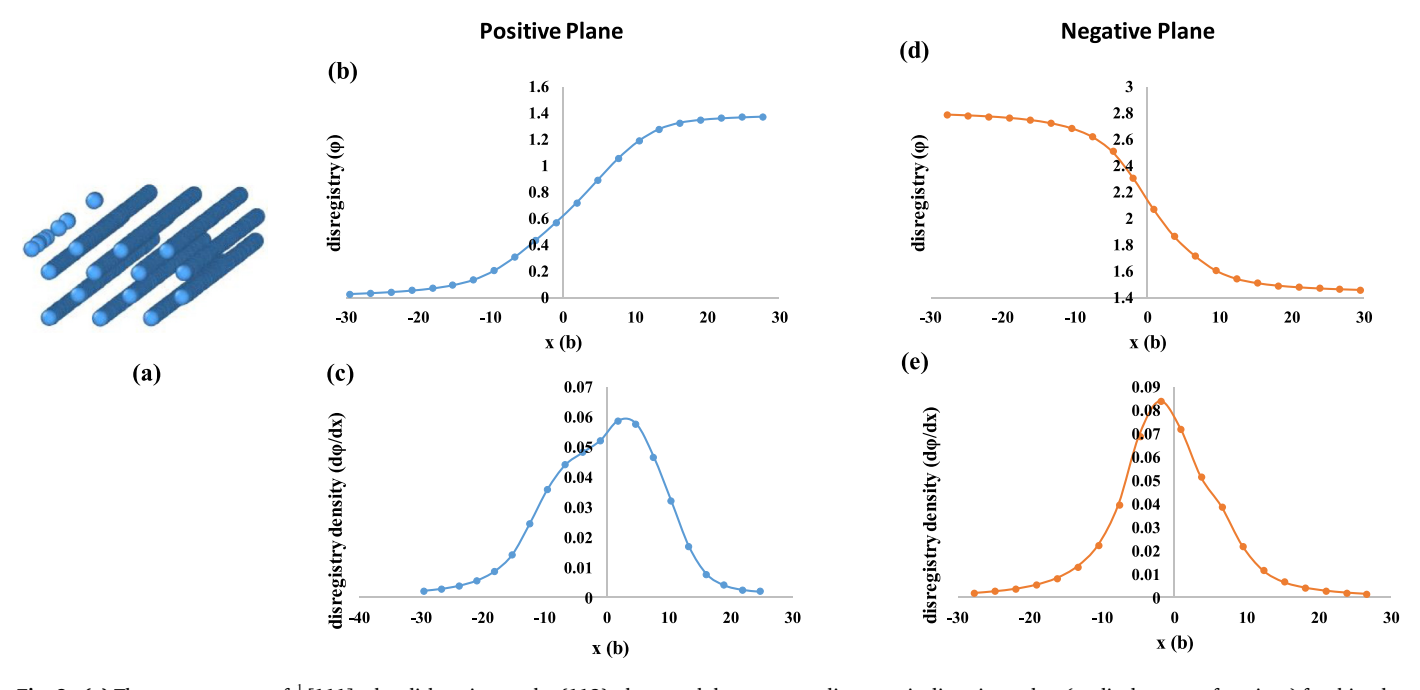


Fig. 8. (a) The core structure of $\frac{1}{2}$ [111] edge dislocation on the {112} plane; and the corresponding atomic disregistry plots (or displacement functions) for this edge dislocation in units of b of atomic layers immediately (b) above (upper layer) and (d) below (lower layer) the (110) slip plane and their corresponding differential misfit plots: (c) above (upper layer) and (e) below (lower layer) the (110) slip plane.

3.3.4. Theoretical predictions of the CRSS

The CRSS of edge dislocations in Ta-8%W alloy can be determine theoretically using the corresponding analytical model for solute strengthening of edge dislocations [7]. According to this model, due to the random nature of solute distribution, the total interaction energies between the dislocations and solute fluctuates as a function of local solute arrangement. Favorable fluctuations in solute concentration can cause the dislocation to be pinned, thus, increasing the barrier for dislocation motion. A theory for the strength of BCC and FCC random alloys was recently derived from the motion of edge dislocation through a random

alloy [61]. A reduced version of this theory predicts zero-temperature shear yield stress and energy barrier for thermally activated flow:

$$\tau_{y0} = A_{\tau} \alpha^{-1/3} \mu_{alloy} \frac{1 + v_{alloy}}{1 - v_{alloy}}^{4/3} \left[\frac{\sum_{n} C_{n} \Delta V_{n}^{2}}{b^{6}} \right]^{2/3}$$
(11)

$$\Delta E_b = A_E \alpha^{1/3} \mu_{alloy} b^3 \frac{1 + v_{alloy}}{1 - v_{alloy}}^{2/3} \left[\frac{\sum_n C_n \Delta V_n^2}{b^6} \right]^{1/3}$$
 (12)

$$\tau_{y}(T,\dot{\epsilon}) = \tau_{y0} \left[1 - \left(\frac{kT}{\Delta E_{b}} \ln \frac{\dot{\epsilon}_{0}}{\dot{\epsilon}} \right) \right]^{2/3}$$
 (13)

Table 4
CRSS for edge dislocations in pure Ta and it's alloys at 5 and 300 K using Zhou EAM and Chen EAM Potential.

Composition	Temperature (K)	CRSS (MPa)	CRSS Analytical Model for Edge Dislocations [40] (MPa)
Ta (Zhou potential)	5K	-	-
	300K	-	-
T111 alloy (Zhou potential)	5K	150-200	197 (MD strain rate)
	300K	80-100	164 (MD strain rate)
Ta (Chen potential)	5K	~ 5	-
		~30 (TD-112)	-
		*~35 (AD-112)	
Ta-8%W (Chen potential)	5K	150 (TD-110)	180 (MD strain rate)
_		200 (AD-110)	
		320 (TD-112)	
		350 (AD-112)	
	300K	120 (TD-110)	178 (MD strain rate)
		180 (AD-110)	

This approximation is based on the assumption that solute/dislocation interaction energy, U_n , of a random alloy with type n-solute is governed by the theory of elasticity (i.e., $U_n = -p\Delta V_n$ where, ΔV_n is the misfit volume of the type n-solute ($n=1,\ldots,N$) in an N-component alloy and p is the pressure field generated by the dislocation at the solute position. Additionally, \dot{e}_0 is the reference strain and is equal to 10^4 s⁻¹, μ_{alloy} is the shear modulus of the alloy, v_{alloy} is the Poisson's ratio, and the value of α is taken as 0.0833 for BCC alloys [15]. The pre-factors A_t and A_E have values of 0.04 and 2.0 for undissociated edge dislocations in BCC alloys. These values are derived from the reduced elasticity theory [7,9] and are hence dependent only on solute misfit volumes and dislocation pressure field. The alloy's elastic constants and the dislocation core structure, in turn, determine the pressure field.

According to this theory, the elastic moduli of the alloy changes slowly with composition, and hence, it is the atomic misfit volumes that play a major role in strengthening. In random alloys with N-components, the misfit volumes ΔV_n of each type-n element $(n=1,\ldots,N)$ is given by:

$$\Delta V_{n} = \frac{\partial V_{alloy}}{\partial C_{n}} - \sum_{m=1}^{N} C_{m} \frac{\partial V_{alloy}}{\partial C_{m}}$$
 (14)

Here, V_{alloy} is the alloy atomic volume and $\partial V_{alloy}/\partial C_n=0$. Here, C_n is the composition of the individual element in the multi-component alloy. In the current study, the alloy misfit volumes have been estimated to be $\Delta V(W)=-2.43~\forall^3$ and $\Delta V(Ta)=0.15~\forall^3$ using molecular static simulations with the Chen potential. A comparison between the CRSS as calculated using this model and those derived from the current atomistic simulations is given in Table 4. For the theoretical calculations, an MD strain rate of $10^6~\rm s^{-1}$ is used. In the current work for edge dislocations in Ta-W alloy, a good agreement is observed between the theoretically predicted CRSS with those predicted from atomistic simulations.

3.4. Dislocation loops

3.4.1. Static equilibrium

The stability of dislocation shear loops at 0 K in Ta-8%W are studied using MD simulations for circular dislocation loops with radii in the range of 50–100 Å. The stability of the dislocation loops was assessed by identifying the minimum constant shear stress in the direction of the Burgers vector required to maintain equilibrium structure of the loop. The results are also compared to the theoretical prediction of the equilibrium stress as derived from the Scattergood and Bacon Eq. (1). This comparison is shown in Fig. 9. It is observed that the equilibrium stress at 0 K as predicted from both simulations and theory are inversely proportional to the loop radius, and that the theoretical and MD predictions are in good agreement with the theoretical ones. Below the critical equilibrium stress, the MD simulations show that the dislocation loops contract, while above it the loops expand.

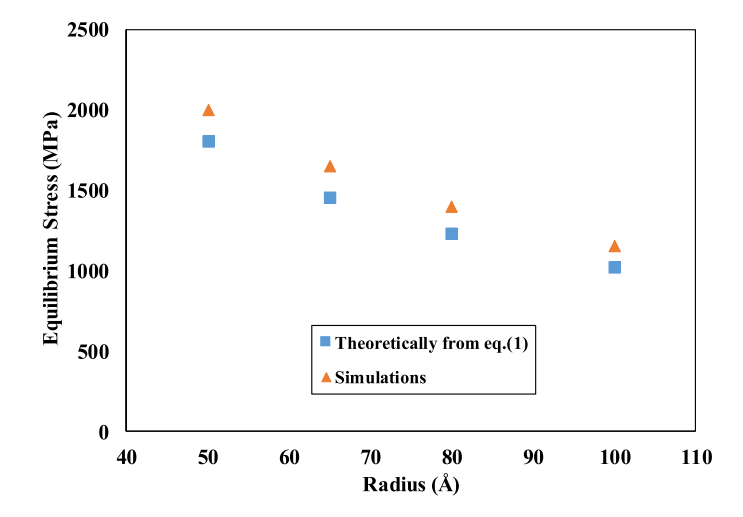


Fig. 9. Equilibrium stresses for loop stability versus the intital dislocation radius in Ta-8%W as predicted from the current MD simulations and from Eq. (1).

3.4.2. Evolution of the dislocation loop under applied shear stress at 5 K

In order to explore the effect of alloying on the shear response of dislocation loops, evolution of the loops under pure shear was studied in pure Ta and Ta-8%W was studied at 5 K. Two types of loop configurations, $\frac{1}{2}$ <111> {110} and $\frac{1}{2}$ <111>{112}, were generated for studying the expansion phenomenon. A loop radius of 10 nm is used for this study. Upon applying a constant shear stress that is higher than this minimum stable shear stress the loops begin to expand. The minimum stress required for the loop to start expanding is closely related to the CRSS of pure edge and screw dislocations, which were estimated previously in the current work. The critical loop equilibrium stress for maintaining a non-expanding, non-contracting stable circular dislocation loop in pure Ta on {110} plane at 5 K is estimated to be 932 MPa from the current atomistic simulations. From our preceding calculations, it was shown that the CRSS for pure Ta in both the twinning and anti-twinning directions for an edge dislocation on {110} planes are symmetric and very small ~5 MPa. Loop expansion of the edge segments of a dislocation loop on the {110} plane in pure Ta starts at 935 MPa. At this instant, the edge segments of the loop experience an excess shear stress of ~5 MPa above the critical loop equilibrium stress and the edge segments in TD and AD start gliding simultaneously in the simulation box. Table 5 summarizes the CRSS for expansion of the dislocation loops along with the CRSS of single edge and screw dislocations in pure Ta on {110} plane. The screw dislocations CRSS in pure Ta is much higher than that of edge dislocations. Therefore, the glide of the screw-oriented segments is initiated at a higher stress of ~1200 MPa. This leads to an elliptical shape of the

Table 5
Details regarding stresses and nature of dislocation loop expansion on {110} plane in pure Ta and Ta-8%W alloy (All stresses are in MPa)

	Equilibrium stress	Edge segment CRSS	CRSS of pure Edge dislocation	Screw segment CRSS	CRSS of pure screw dislocation	Nature of expansion-edge portion	Nature of expansion-screw portion
Pure Ta	932	935	5	1200	400	Symmetrical	Symmetrical
Ta-8%W alloy	1000	1200	150 TD	1600	600	Symmetrical	Symmetrical with cross
			200 AD				kink motion

Table 6
Details regarding the CRSS and nature of loop expansion on {112} plane in pure Ta and Ta-8%W alloy (All stresses are in MPa)

	Equilibrium stress (MPa)	Edge segment CRSS	CRSS of pure Edge dislocation	Screw segment CRSS	Nature of expansion-edge portion	Nature of expansion-screw portion
Pure Ta	980	1110	30 – TD 35 - AD	1110	Symmetrical	Symmetrical
Ta-8%W alloy	1000	1300	TD - 320	1600 (for a screw dislocation on {110} plane)	Symmetrical	Symmetrical with cross kinks and movement glide on {112} plane

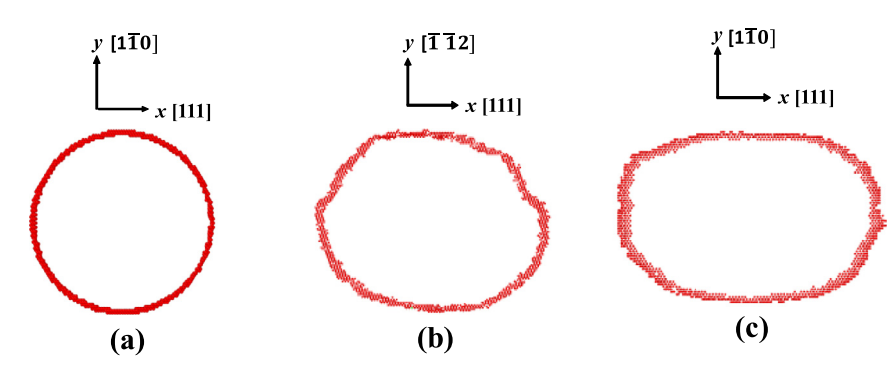


Fig. 10. Equilibrium shape of a dislocation loop on the: (a) $\{112\}$ plane in pure Ta; (b) $\{110\}$ plane in Ta-8%W; and (c) $\{112\}$ plane in Ta-8%W.

expanding loop, as shown in Fig. 11(a). Similar behavior is observed during the expansion of the dislocation loop lying on the $\{112\}$ plane in pure Ta. The CRSS corresponding to the dislocation loop in Ta lying on the $\{112\}$ plane is summarized in Table 6. We observe from the values quoted in Table 6 that the equilibrium stress for a stable circular loop on the $\{112\}$ plane in pure Ta is ~ 980 MPa. The edge portion of the loop exhibits expansion at a stress of ~ 1110 MPa. This is around ~ 30 MPa above the corresponding equilibrium stress (980 MPa), and is close to the CRSS of an isolated pure edge dislocation on the $\{112\}$ plane in Ta (i.e., 30-35 MPa).

A change in the loop expansion was observed after the addition of alloying element and is explained in the following. The first feature that distinguishes the loop expansion phenomenon in pure Ta from that of Ta-8%W is the rugged nature of the equilibrium loop shapes. These equilibrium shapes of the dislocation loops in Ta on {112} plane and Ta-8%W alloy on the {110} and {112} planes are compared in Fig. 10. The second feature is the change in CRSS required for loop expansion in pure Ta and Ta-8%W alloys. Tables 5 and 6 give the CRSS for the dislocation loops in Ta-8%W generated on the {110} and {112} planes. The equilibrium stress for a 10 nm circular loop in Ta-8%W on the {110} plane is ~1000 MPa, while the CRSS for a single edge dislocation in Ta-8%W at 5 K has ~200-250 MPa. At a stress of ~1200 MPa (which is \sim 200 MPa above the equilibrium stress for the stable loop), the edge segments of the loop begin to expand and glide completely out of the simulation box. At this stress, a slight movement is also observed in the screw segment but given the higher CRSS of the isolated screw dislocation, this glide is intuitively limited. These simultaneous events give an elliptical shape to the loop during expansion (Fig. 11(b)). At a shear stress of 1500-1600 MPa the glide of screw segments of the loop is initiated. This can be reasoned by the high CRSS of a pure screw dislocation lying on the {110} planes at 5 K in the alloy, which has already been established to be ~600 MPa. Thus, even though the equilibrium stress

for maintaining a circular dislocation loop in Ta and Ta-8%W are not significantly different, the CRSS values for loop expansion vary remarkably. This can be directly correlated to the notable difference in stress required to glide an isolated edge and screw dislocation segments in Ta and Ta-8%W.

Apart from the difference in the equilibrium shapes and CRSS of the dislocation loop, in pure Ta and Ta-8%W, the third distinguishing feature is comparatively rough glide paths in Ta-8%W. Fig. 11 shows an expanding $\frac{1}{2}{<}111{>}\{112\}$ loop in pure Ta under a constant shear stress of ${\sim}1100$ MPa and $\frac{1}{2}{<}111{>}\{110\}$ loop in Ta-8%W under a constant shear stress of ${\sim}1200$ MPa. The edges of the loop appear jagged in Ta-8%W whereas in pure Ta the loop edges are pretty smooth even during expanding. This rugged shape and roughened glide of the loops in the alloy could be attributed to local trapping and de-trapping of the dislocation segments due to the presence of alloying sites.

A 3D view of the loop as it glides post expansion and breaks down into individual screw and edge segments is also shown in Fig. 12. Here, we can see that as the loop expands, the two screw portions begin to move on the {112} planes. This effective glide of screw dislocation on {112} planes could be an artefact of the interatomic potential as has been explained in detail in the previous sections. The movement of screw segment of the $\frac{1}{2} < 111 > \{110\}$ loop leaves behind debris, while transcending onto the $\{112\}$ planes. This is analogous to the sequence of events observed during the glide of a single infinitely long screw dislocation in these alloys.

The nature of expansion of the $\frac{1}{2}$ <111>{112} loop is also similar to the $\frac{1}{2}$ <111>{110} loop. In our preceding calculations, it was established that the CRSS of the edge dislocations lying on the {112} planes are higher in comparison to the one on the {110} plane. Innately, expansion of the edge portion of the $\frac{1}{2}$ <111>{112} shear dislocation loop is initiated at higher applied shear stresses when compared to the $\frac{1}{2}$ <111>{110} loop. These values compared in Tables 5 and 6.

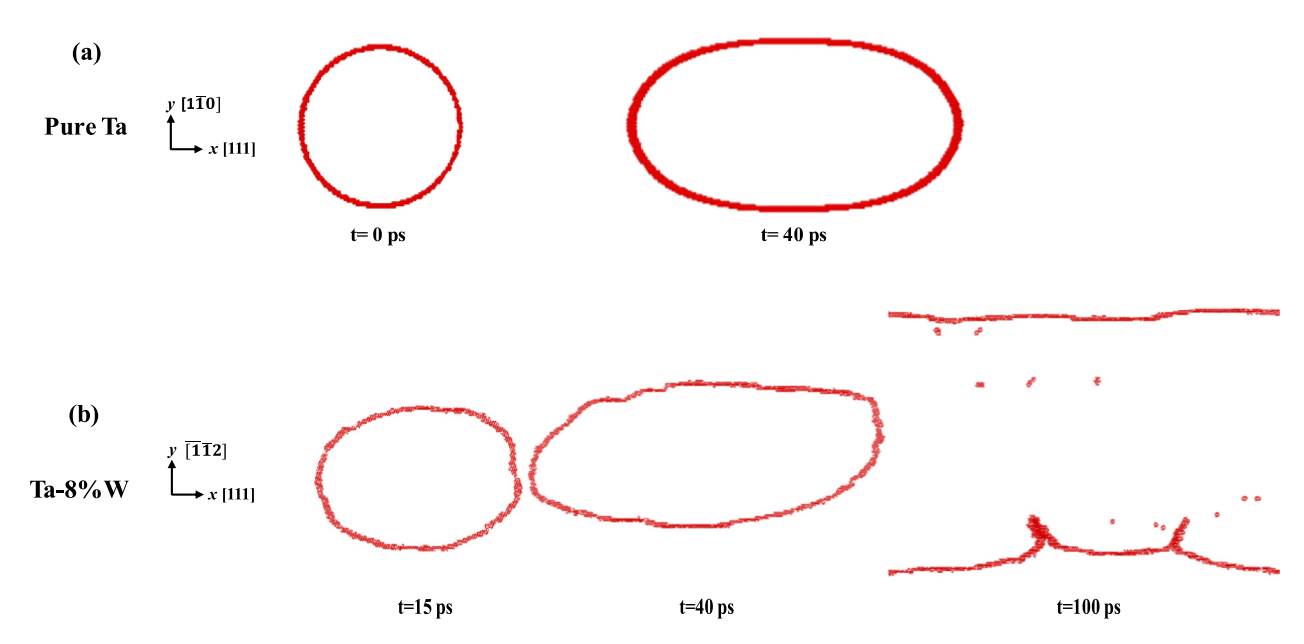


Fig. 11. (a) Smooth glide of the edge and screw segments of a {112} dislocation loop in pure Ta at 1110 MPa and 5 K at two time-steps. (b) Rugged glide of edge and screw segments of a {110} dislocation loop in Ta-8%W alloy at 1200 MPa and 5 K at three time-steps.

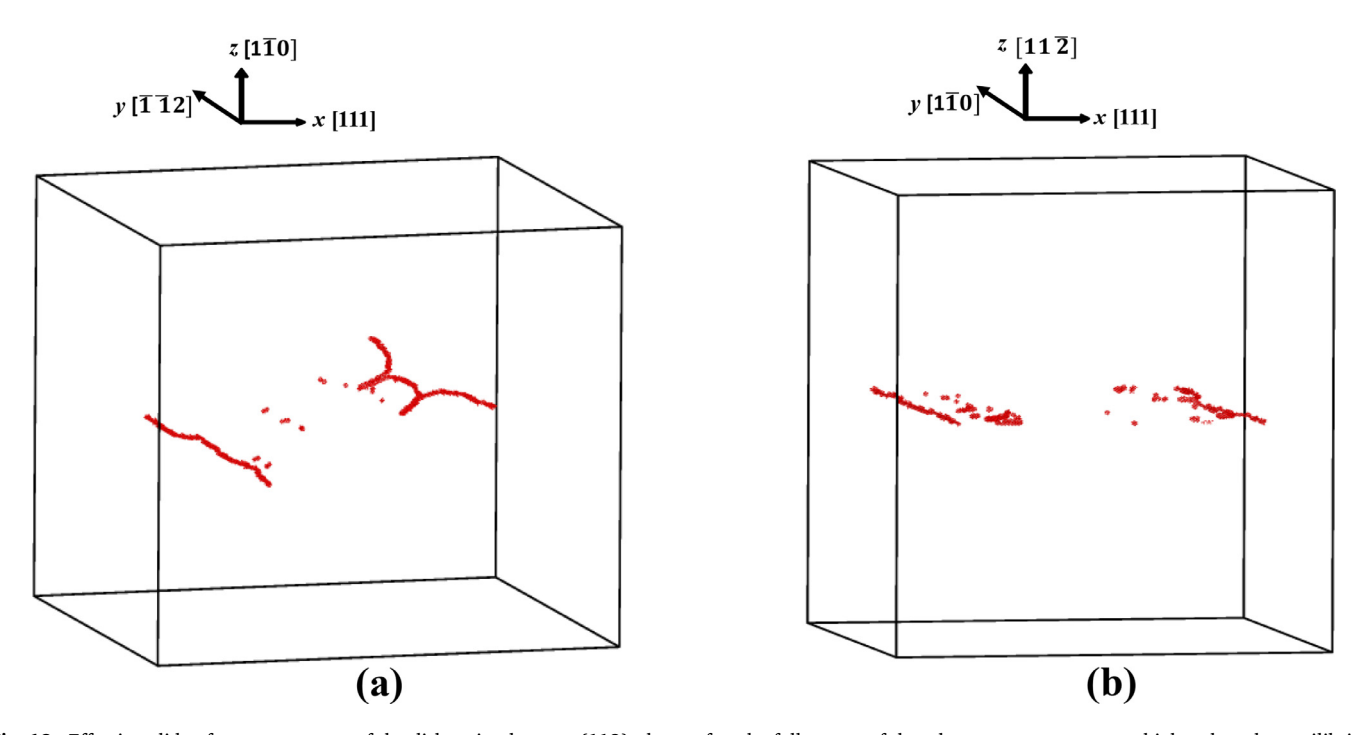


Fig. 12. Effective glide of screw segments of the dislocation loop on {112} planes after the full escape of the edge segments at stresses higher than the equilibrium stresses of a loop initially lying on the: (a) 110; and (b) 112 plane.

4. Summary and conclusions

The effect of alloying Ta with small amounts of W on the dislocation core structure, critical resolved shear stress and mobility of $\frac{1}{2}{<}111{>}$ screw and edge dislocations in Ta-8%W alloy was studied using molecular statics and dynamics simulations at 5 and 300 K using the Chen EAM potential. The CRSS for screw dislocations in Ta-8%W with the Chen potential was estimated to be 600 MPa and 300 MPa for screw dislocations at 5 K and 300 K, respectively, under MD strain rate conditions. A theoretical model of screw dislocation governed plasticity in BCC alloys (Rao-Suzuki model) was used to determine the CRSS of $\frac{1}{2}$

[111] screw dislocations Ta based alloys at the given temperature (5 and 300 K) and MD strain rates. A good agreement is found between the CRSS values obtained through simulations and the Rao-Suzuki model predictions. W solute – screw dislocation interaction energy in pure Ta as obtained from the Chen potential was used in the model calculations. In addition, this theoretical model BCC was also used to determine the CRSS of $\frac{1}{2}$ [111] screw dislocations in Ta based alloys as a function of temperature (room temperature to 1600 $^{\rm o}$ C). The CRSS shows a slower decrease with increasing temperature in Ta-8%W as compared to simple BCC metals. These predictions obtained at an experimental strain rate of 0.001 $\rm s^{-1}$ was compared with experimental yield data for temperatures

ranging from room temperature to $1600\,^{\circ}$ C. First principles W solute – screw dislocation interaction energy data for pure Ta was used in these calculations.

Local chemical variations due to presence of random solutes also substantially increase the CRSS of edge dislocations in the alloy when compared to that of pure Ta. In pure Ta, the CRSS for edge dislocations is very small ~5–35 MPa, depending upon the dislocation glide plane, in pure Ta. The investigation of CRSS of edge dislocation in pure Ta and Ta-8%W led to some interesting insights about shear stress asymmetry in the alloys in twinning and anti-twinning direction. Since TD-AD asymmetry is not observed in pure Ta, it is most likely induced by alloying Ta with W. The irregularity observed in atomic disregistry or differential misfits and differential displacement plots for edge dislocations in Ta-8%W on both {110} and {112} planes explain the difference in AD and TD CRSS.

Finally, stability and expansion of shear dislocation loops were also studied for the Ta-W alloy. Theoretical results for loop stabilizing stress from Scattergood and Bacon's equation were in agreement with those obtained from direct atomistic simulations. The loop expansion results were in accord with straight dislocation CRSS estimates.

Declaration of Competing Interest

The authors declare that they have no known competing financial interests or personal relationships that could have appeared to influence the work reported in this paper.

Acknowledgment

This work was supported by the U.S. National Science Foundation (NSF) award number DMR-1807708. The authors also acknowledge computational resources at the Maryland Advanced Research Computing Center (MARCC). This work was partially carried out at the Advanced Research Computing at Hopkins (ARCH) core facility (rockfish.jhu.edu), which is supported by the NSF grant #OAC-1920103. This work was also partially carried out on Expanse at the San Diego Supercomputing Center through allocation TG-MAT210003 using Extreme Science and Engineering Discovery Environment (XSEDE) [62], which is supported by NSF grant number ACI-1548562.

References

- B. Chen, S. Li, H. Zong, X. Ding, J. Sun, E. Ma, Unusual activated processes controlling dislocation motion in body-centered-cubic high-entropy alloys, Proc. Natl. Acad. Sci. U. S. A. 117 (28) (2020) 16199–161206.
- [2] S.I. Rao, C. Woodward, T.A. Parthasarathy, O. Senkov, Atomistic simulations of dislocation behavior in a model FCC multicomponent concentrated solid solution alloy, Acta Mater. 134 (2017) 188–194.
- [3] S.I. Rao, C. Woodward, B. Akdim, O.N. Senkov, A model for interstitial solid solution strengthening of body centered cubic metals, Materialia 9 (2020) 100611.
- [4] J. Christian, Some surprising features of the plastic deformation of body-centred cubic metals and alloys. [Campbell Memorial Lecture, ASM, 1982.], Metall. Trans. A 14 (1983) 1237–1256.
- [5] M.S. Duesbery, V. Vitek, Optical birefringence, Acta Metall. 1 (5) (2012) 1481–1492.
- [6] S.I. Rao, C. Woodward, B. Akdim, O.N. Senkov, D. Miracle, Theory of solid solution strengthening of BCC chemically complex alloys, Acta Mater. 209 (2021) 116758.
- [7] F. Maresca, W.A. Curtin, Mechanistic origin of high strength in refractory BCC high entropy alloys up to 1900 K, Acta Mater. 182 (2020) 235–249.
- [8] S. Plimpton, Short-range molecular dynamics, J. Comput. Phys. 117 (6) (1997) 1–42.
- [9] https://www.ctcms.nist.gov/potentials/
- [10] Y. Chen, et al., Development of the interatomic potentials for W-Ta system, Comput. Mater. Sci. 163 (December 2018) (2019) 91–99.
- [11] A. Stukowski, Visualization and analysis of atomistic simulation data with OVI-TO-the open visualization tool, Model. Simul. Mater. Sci. Eng. 18 (1) (2010).
- [12] S.I. Rao, C. Varvenne, C. Woodward, T.A. Parthasarathy, D. Miracle, O.N. Senkov, W.A. Curtin, Atomistic simulations of dislocations in a model BCC multicomponent concentrated solid solution alloy, Acta Mater. 125 (2017) 311–320.
- [13] P. Hirel, Atomsk: a tool for manipulating and converting atomic data files, Comput. Phys. Commun. 197 (2015) 212–219.
- [14] R.O. Scattergood, D.J. Bacon, Dislocation shear loops in anisotropic crystals, Phys. Status Solidi 25 (2) (1974) 395–404.
- [15] A. Dewaele, P. Loubeyre, M. Mezouar, Refinement of the equation of state of tantalum. Phys. Rev. B 69 (2004) 092106.
- [16] D.E. Gray, American Institute of Physics Handbook, McGraw-Hill, New York, 1957.

- [17] F.H. Featherston, J.R. Neighbours, Elastic constants of tantalum, tungsten, and molybdenum. Phys. Rev. 130 (1963) 1324–1333.
- [18] K.W. Katahara, M.H. Manghnani, E.S. Fisher, Pressure derivatives of the elastic moduli of BCC Ti-V-Cr, Nb-Mo and Ta-W alloys, J. Phys. F Met. Phys. 9 (1979) 773– 791.
- [19] C.T. Liu, H. Inouye, R.W. Carpenter, Mechanical Properties and Structure of Oxygen-Doped Tantalum-Base Alloy, Oak Ridge National Laboratory, 1972.
- [20] C.E. Anderson, F.R. Brotzen, Elastic constants of tantalum-tungsten alloys, J. Appl. Phys. 53 (1982) 292.
- [21] C. Bercegeay, S. Bernard, First-principles equations of state and elastic properties of seven metals, Phys. Rev. B 72 (2005) 214101.
- [22] L. Koci, Y. Ma, A.R. Oganov, et al., Elasticity of the superconducting metals V, Nb, Ta, Mo, and W at high pressure, Phys. Rev. B 77 (2008) 214101.
- [23] M. Foata-Prestavoine, G. Robert, M.H. Nadal, et al., First-principles study of the relations between the elastic constants, phonon dispersion curves, and melting temperatures of BCC Ta at pressures up to 1000 GPa, Phys. Rev. B 76 (2007) 104104.
- [24] F. Mouhat, F.X. Coudert, Necessary and sufficient elastic stability conditions in various crystal systems, Phys. Rev. B Condens. Matter Mater. Phys. 90 (22) (2014) 4–7.
- [25] S.I. Rao, B. Akdim, E. Antillon, C. Woodward, T.A. Parthasarathy, O.N. Senkov, Modeling solution hardening in BCC refractory complex concentrated alloys: nbTiZr, Nb 1.5 TiZr 0.5 and Nb 0.5 TiZr 1.5, Acta Mater. 168 (2019) 222–236.
- [26] C. Woodward, S.I. Rao, Flexible Ab Initio Boundary conditions: simulating isolated dislocations in BCC Mo and Ta, Phys. Rev. Lett. 88 (21) (2002).
- [27] L. Romaner, C. Ambrosch-Draxl, R. Pippan, Effect of rhenium on the dislocation core structure in tungsten, Phys. Rev. Lett. 104 (2010) 195503.
- [28] L. Ventelon, F. Willaime, E. Clouet, D. Rodney, Ab initio investigation of the Peierls potential of screw dislocations in BCC Fe and W, Acta Mater. 61 (2013) 3973–3985.
- [29] C.R. Weinberger, G.J. Tucker, S.M. Foiles, Peierls potential of screw dislocations in BCC transition metals: predictions from density functional theory, Phys. Rev. B 87 (2012) 1.0
- [30] L. Dezerald, L. Ventelon, E. Clouet, C. Denoual, D. Rodney, F. Willaime, Ab initio modeling of the two-dimensional energy landscape of screw dislocations in BCC transition metals, Phys. Rev. B 89 (2014) 1–13, doi:10.1103/PhysRevB.89.024104.
- [31] C.R. Weinberger, B.L. Boyce, C.C. Battaile, Slip planes in BCC transition metals, Int. Mater. Rev. 58 (5) (2013) 296–314.
- [32] L. Dezerald, L. Ventelon, E. Clouet, C. Denoual, D. Rodney, F. Willaime, Ab initio modeling of the two-dimensional energy landscape of screw dislocations in BCC transition metals, Phys. Rev. B Condens. Matter Mater. Phys. 89 (2) (2014) 1–13.
- [33] L. Ventelon, F. Willaime, Generalized stacking-faults and screw- dislocation core-structure in BCC iron: a comparison between ab initio calculations and empirical potentials, Philos. Mag. 90 (7–8) (2010) 1063–1074.
- [34] G. Wang, et al., Molecular dynamics simulations of 1/2 a<1 1 1 > screw dislocation in Ta, Mater. Sci. Eng. A309–310 (2001) 133–137.
- [35] K. Ito, V. Vitek, Atomistic study of non-Schmid effects in the plastic yielding of BCC metals, Philos. Mag. A 81 (5) (2001) 1387–1407.
- [36] G.J. Ackland, R. Thetford, An improved N-body semi-empirical model for body-centred cubic transition metals, Philos. Mag. A 56 (1) (1987) 15-3.
- [37] Ab initio study of screw dislocations in Mo and Ta: a new picture of plasticity in BCC transition metals, Phys. Rev. Lett. 84 (7) (2000).
- [38] M.W. Finnis, J.E. Sinclair, A simple empirical N-body potential for transition metals, Philos. Mag. A 50 (1984) 45–55.
- [39] G.J. Ackland, R. Thetford, An improved N-body semi-empirical model for body-centred cubic transition metals, Philos. Mag. A 56 (1987) 15–30.
 [40] Y. Mishin, A.Y. Lozovoi, Angular-dependent interatomic potential for tantalum, Acta
- [40] Y. Mishin, A.Y. Lozovoi, Angular-dependent interatomic potential for tantalum, Acta Mater. 54 (2006) 5013–5026.
- [41] F. Maresca, D. Dragoni, G. Csányi, et al., Screw dislocation structure and mobility in body centered cubic Fe predicted by a Gaussian approximation potential, NPJ Comput. Mater. 4 (69) (2018).
- [42] C. Woodward, S.I. Rao, Flexible Ab initio boundary conditions: simulating isolated dislocations in BCC Mo and Ta, Phys. Rev. Lett. 88 (2002) 216402.
- [43] S.I. Rao, C. Woodward, Atomistic simulations of (a/2)(111) screw dislocations in BCC Mo using a modified generalized pseudopotential theory potential, Philos. Mag. A 81 (5) (2001) 1317–1327.
- [44] J.J. Möller, E. Bitzek, BDA: a novel method for identifying defects in body-centered cubic crystals, MethodsX 3 (2016) 279–288.
- [45] J. Marian, W. Cai, V.V. Bulatov, Dynamic transitions from smooth to rough to twinning in dislocation motion, Nat. Mater. 3 (3) (2004) 158–163.
- [46] M.H.A. Nawaz, B.L. Mordik, Slip geometry of tantalum and tantalum alloys, Phys. Status Solidi 32 (1975) 449.
- [47] C.R. Weinberger, B.L. Boyce, C.C. Battaile, Slip planes in BCC transition metals, Int. Mater. Rev. 58 (5) (2013) 296–314.
- [48] M.S. Duesberyr, A. Foxallan, P.B. Hirsch, The plasticity of pure niobium single crystals, J. Phys. Colloq. 27 (C3) (1966) 193–204.
- [49] L.M. Hale, J.A. Zimmerman, C.R. Weinberger, Simulations of BCC tantalum screw dislocations: why classical inter-atomic potentials predict {1 1 2} slip, Comput. Mater. Sci. 90 (2014) 106–115.
- [50] edited by H. Suzuki, F.R.N. Nabarro, Solid-solution hardening in body-centered cubic alloys, in: Dislocations in Solids, 4, North Holland, Amsterdam, 1965, p. 191. edited by.
- [51] H. Suzuki, Solid solution hardening, in: Strength of Metals and Alloy', Proceedings of the 5th International Conference, Aachen, Federal republic of Germany, 3, Pergamon Press. New York, 1979, p. 1595.
- [52] H.R. Hattendorf, A. Buchner, Plastic behavior of FeP single crystals, Z. Metallkd. 81 (1990) 739.
- [53] A.R. Buchner, W. Wunderlich, A new discussion of the interaction energy in the solid solution hardening of BCC iron alloys, Phys. Status Solidi 135 (1993) 391.

- [54] H.R. Hattendorf, A. Buchner, A review of Suzuki's solid solution hardening theory for substitutional BCC alloys, Z. Metallkd. 83 (1992) 9.
- [55] F. Louchet, B. Viguier, Ordinary dislocations in γ -TiAl: cusp unzipping, jog dragging and stress anomaly, Philos. Mag. A 80 (4) (2000) 765.

 [56] P.M. Derlet, D. Nguyen-Manh, S.L. Dudarev, Multiscale modeling of crowdion and
- vacancy defects in body-centered-cubic transition metals, Phys. Rev. B Condens. Matter Mater. Phys. 76 (5) (2007) 1–22.
- [57] S.M. Foiles, "Local varability of the Peierls barrier of screw dislocations in Ta-10W", Sandia Report, SAND2017-11595, Unlimited Release, Printed October 2017.

 [58] R.E Peierls, The size of a dislocation, Proc. Phys. Soc. 52 (1940) 23.

 [59] F.R.N Nabarro, Dislocations in a simple cubic lattice, Proc. Phys. Soc. 59 (1947) 256.

- 2} edge dislocation in BCC iron studied by molecular dynamics, Acta Mater. 57 (5) (2009) 1416–1426.
- [61] B. Yin, F. Maresca, W.A. Curtin, Vanadium is an optimal element for strengthening
- in both FCC and BCC high-entropy alloys, Acta Mater. 188 (2020) 486–491.

 [62] J. Towns, T. Cockerill, M. Dahan, I. Foster, K. Gaither, A. Grimshaw, V. Hazlewood, S. Lathrop, D. Lifka, G.D. Peterson, R. Roskies, J.R. Scott, N. Wilkins-Diehr, XSEDE: accelerating scientific discovery, Comput. Sci. Eng. 16 (2014) 62–74.
- [63] S. Takeuchl, K. Maeda, Slip in high purity tantalum between 0.7 and 40 K, Acta Metall. 25 (1977) 1485–4190.